ISSN 1990-3413, Astrophysical Bulletin, 2022, Vol. 77, No. 4, pp. 397–406. © Pleiades Publishing, Ltd., 2022.
Russian Text © The Author(s), 2022, published in Astrofizicheskii Byulleten', 2022, Vol. 77, No. 4, pp. 441–451.

Kinematics and Origin of Gas in the Disk Galaxy NGC 2655

O. K. Sil'chenko[a], *, A. V. Moiseev[a, b], **, A. S. Gusev[a], *, and D. V. Kozlova[c]**

[a] *Sternberg Astronomical Institute, Lomonosov Moscow State University, Moscow, 119234 Russia*
[b] *Special Astrophysical Observatory, Russian Academy of Sciences, Nizhnii Arkhyz, 369167 Russia*
[c] *Leibniz-Institut für Astrophysik (AIP), Ander Sternwarte 16, 14482 Potsdam, Germany*
**e-mail: olga@sai.msu.su*
***e-mail: moisav@gmail.com*
****e-mail: gusev@sai.msu.ru*

Received August 24, 2022; revised September 29, 2022; accepted September 30, 2022

Abstract—The new observational data concerning distribution, excitation, and kinematics of the ionized gas in the giant early-type galaxy NGC 2655 obtained at the 6m telescope of the Special Astrophysical Observatory (SAO RAS) and at the 2.5 m telescope of the Caucasian Mountain Observatory (CMO SAI MSU) are presented in this work. The joint analysis of these and earlier spectral observations has allowed us to make a conclusion about multiple nature of the gas in NGC 2655. Together with a proper large gaseous disk experiencing regular circular rotation in the equatorial plane of the stellar potential of the galaxy for billions years, we observe also remnants of a merged small satellite having striked the central part of NGC 2655 almost vertically for some 10 million years ago.

Keywords: galaxies: early-type, galaxies: evolution, galaxies: star formation, galaxies: individual: NGC2655
DOI: 10.1134/S1990341322040137

1. INTRODUCTION

The morphological type of lenticular galaxies was introduced by Hubble (1936) as a transitional type from elliptical to spiral galaxies. However, in the presence of a large-scale stellar disk in their structure, lenticular galaxies did not show noticeable star formation in it. In the early days of extragalactic astronomy development, a natural hypothesis was made that star formation does not occur in the disks of lenticular galaxies, because there is no gas there; and the gas is not there, because it was somehow "removed", for example, by interaction with the hot intergalactic medium in a cluster (Gunn and Gott, 1972; Larson et al., 1980). However, since then the paradigm of the spiral (disk) galaxy evolution has changed, it became clear that the entire evolution of disk galaxies is accompanied by an inflow of cold gas from outside compensating for any losses of it in the disk, in particular, the losses due to star formation (Tacconi et al., 2020). Also, deep radio observations, both blind surveys like ALFALFA (Grossi et al., 2009) and targeted studies of specific samples of early-type galaxies, such as the ATLAS-3D survey (Serra et al., 2012), showed that almost half of the field lenticular galaxies has massive extended gaseous disks. Why does not the same star formation take place in these disks as that in the disks of spiral galaxies?

Studies of gas kinematics in field lenticular galaxies have always shown impressive percentage of mismatched rotation of gas and stars—from 24% (Kuijken et al., 1996) in earlier papers up to 36% (Davis et al., 2011) and even up to half of all lenticular galaxies in the extremely rarefied environment (Katkov et al., 2015). We have made an assumption that the suppressed star formation in gas-rich lenticular galaxies may be due to the oblique inflow of the accretion flow: the gas falling angle-wise into the potential well of the stellar disk forms shock waves, heats up, and becomes unable to form stars. We tested this hypothesis with a sample of 18 lenticular galaxies with the extended gaseous disks observing them with a panoramic spectrograph, the Fabry–Perot scanning interferometer of the 6-m SAO RAS telescope, constructing 2D line-of-sight velocity maps, and tracing the orientation of the rotating gas in space with a change in the orientation angles along the galaxy's radius. Indeed, star formation (star formation rings in lenticular galaxies) appeared to be noticeable only at those radii, where the gas lies onto the plane of the stellar disk. While in inclined gaseous disks, star formation does not proceed (Sil'chenko et al., 2019).

One of the objects in our sample in the paper by Sil'chenko et al. (2019) was a nearby giant lenticular galaxy NGC 2655. Figure 1 presents its images: both from the ground-based photometric observations of the BASS survey and high spatial resolution composite images from the Hubble space telescope.

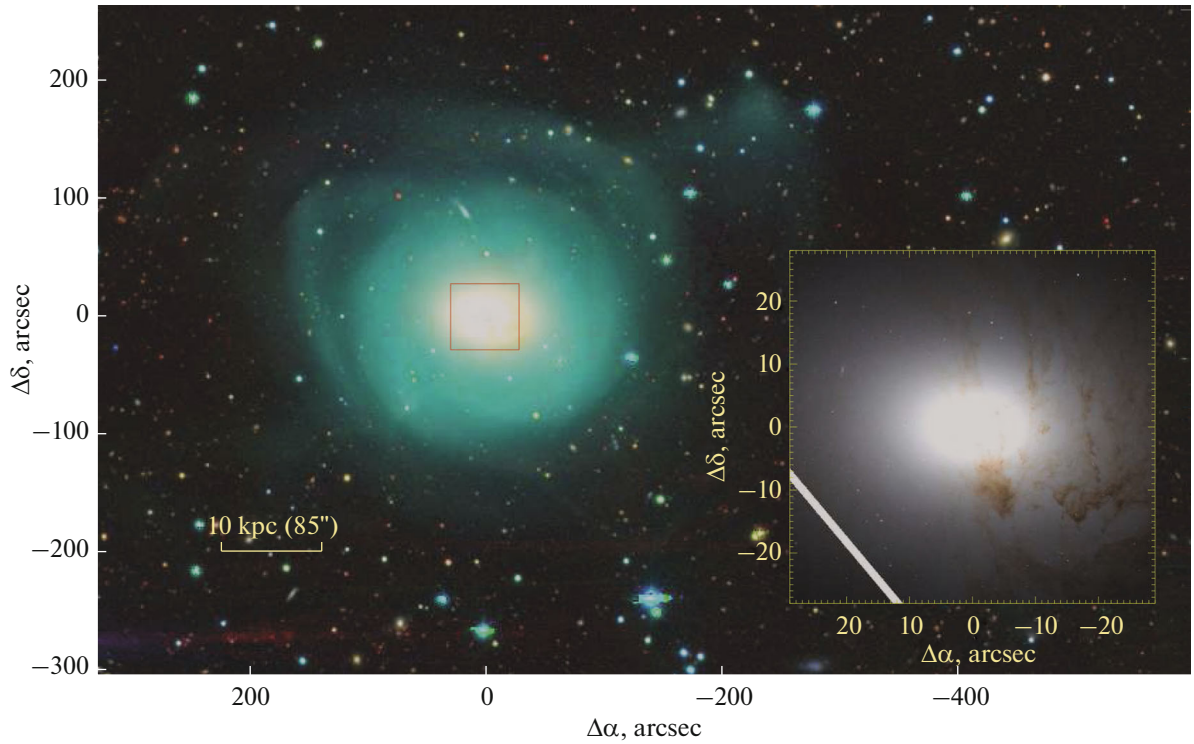

Fig. 1. Image of NGC 2655 in optical colors according to the DESI Legacy Imaging Surveys. The inset shows the central part of the galaxy according to the data from the WFC3 camera of the Hubble Space Telescope (the combined images in the F814W and F555W filters). Asymmetric dust rings from the circumnuclear gaseous disk can be observed.

NGC 2655 is a giant disk galaxy in the center of the group: at a currently accepted distance to the galaxy of 24.4 Mpc (the scale is 118 pc/arcsec), its absolute magnitude $M_K = -25^m$ (LEDA and NED), and the mass of the stellar population is $2\times10^{11} M_\odot$ (Bouquin et al., 2018). The group includes 6–7 galaxies brighter than $M_B = -15^m$, all of them are of the late type (Garcia, 1993). With this configuration, one would expect that the whole gaseous content of NGC 2655 could result from merging of the group's dwarf members by the central galaxy. Indeed, NGC 2655 is abundant in neutral hydrogen: since the earliest surveys, up to 3–6 billion solar masses of neutral hydrogen (Lewis and Davies, 1973) have been found in the galaxy; it forms a disk with a diameter of five times the diameter of the stellar disk (Huchtmeier and Richter, 1982). The integral star formation rates estimated from the ultraviolet image of the galaxy according to the data from the GALEX space telescope is 0.08 $M_\odot$ per year (Bouquin et al., 2018), which places the galaxy significantly below the Main Sequence classifying it as a "galaxy with suppressed star formation" (Cortese et al., 2020). At the same time, it should be noted that such star formation rates are anomalously low for the observed abundance of H I (Catinella et al., 2018). Mapping the distribution of the density of neutral hydrogen (Shane and Krumm 1983; Sparke et al., 2008) reveals the elongation of the projected gaseous disk in a position angle of approximately 110; the relation of this orientation with the parameters of the orientation of the stellar disk plane will be the subject of a detailed discussion in our paper. As for the kinematics of stars and gas, mapped for the central part of the galaxy with panoramic spectroscopy, the gas demonstrates a polar rotation in the center with respect to the stars (Dumas et al., 2007; Sil'chenko and Afanasiev, 2004).

Another point to dwell on is the active nucleus of NGC 2655. Most researchers following us (Sil'chenko and Burenkov, 1990) consider the nucleus of NGC 2655 to be the Seyfert type II but, for example, Keel and Hummel (1988) noted a strong emission of [O I] λ 6300 in the nucleus spectrum and classified it as LINER. The NGC 2655 nucleus shows a noticeable flux in X ray including hard X ray (Terashima et al., 2002). High resolution mapping of the NGC 2655 nucleus in the radio continuum detects a source with a steep spectrum compact both at wavelengths of 6 cm and 20 cm (Hummel et al., 1984); and from the nuclear source in the "west–east" direction, a double-way jet comes out and eventually curves closer to the "north–south" direction (Ho and Ulvestad, 2001). Perhaps it is the jet that excites another compact radio source at 15″ southeast of the nucleus with the same steep spectrum as that of the nucleus (Keel and Hummel, 1988).

NGC 2655 is a case of highly inclined rotation of gas in the absence of any evidence of star formation, which is of particular interest to us as a classic case of a lenticular galaxy with a large gaseous disk. However, the large-scale pattern of the velocity distribution in the extended gaseous disk of NGC 2655 cannot be explained within a simple geometric model of an inclined rotation plane. Both the velocities and the brightness distribution of the emission lines in this galaxy reveal a very complex pattern. We have made some additional observations and are now ready to look into the details of how and when the gas entered NGC 2655.

2. NEW OBSERVATIONS

We have already devoted several papers to the galaxy NGC 2655 (Sil'chenko and Afanasiev, 2004; Sil'chenko and Burenkov, 1990; Sil'chenko et al., 2019) and we have a rich set of the observed spectroscopic data obtained earlier with the 6-m BTA telescope. However, some incomprehensible moments remained in the interpretation of the ionized gas kinematics and, in order to work with them, we decided to obtain additionally observed data.

2.1. Mapping in Emission Lines

We obtained an image of the galaxy with the NBI camera (Shatsky et al., 2020) in a narrow Halp filter centered on the complex of bright ionized gas emission lines Hα+ [N II] λ 6548, λ 6583 with the 2.5-m telescope of the Caucasus Mountain Observatory of SAI MSU (Shatsky et al., 2020) on January 10, 2018. The seeing during the observations was $2\farcs5$. The center wavelength of the filter used was 6560 Å, the bandwidth was 77 Å, so both the [N II] λ 6548, λ 6583 doublet lines and the hydrogen Balmer line fell there. At the same time, a feature of NGC 2655 is that the [N II] λ 6583 line is stronger than the Hα line throughout the body of the galaxy (Sil'chenko and Burenkov, 1990). The total exposure of the analyzed galaxy image in the emission lines was 25 minutes. The image scale was $0\farcs155$ per pixel. In addition to photometry in the narrow Halp filter, the galaxy was also exposed in the neighboring continuum for 20 minutes (through the filter with a width of 100 Å centered on λ 6430 Å), so that after subtracting the image in the continuum from the image obtained in the Halp filter, it would be possible to obtain a proper intensity distribution of the emission lines. Figure 2 shows the result of this procedure together with the $g-r$ color map calculated from the broadband photometry in the BASS survey[1]. The morphology of the image in the emission lines represents a narrow loop, the center of which does not coincide with the center of the galaxy, plus a compact emission region in $15''$ southeast of the nucleus, which was previously detected in radio emission in the continuum (indicated in our picture as ESE). A dusty (red) loop outlines the inner edge of the gas emission loop and is especially brightly visible to the south of the center of NGC 2655. It is apparently associated with shock fronts generated by the collision of an inclined nuclear gaseous disk with proper galaxy's gas, probably lying in the main plane of the galactic disk: the gas is compressed in shock fronts, and the dust associated with it manifests itself as narrow red lanes on color maps. Similar features can be clearly seen, for example, on the edges of strong bars in spiral galaxies.

[1] The data are provided by the DESI Legacy Imaging Surveys website legacysurvey.org.

2.2. Long-Slit Spectroscopy

Additional long-slit spectroscopic data were obtained on May 26, 2022 at the BTA, the 6-m SAO RAS telescope, with the SCORPIO-2 multi-mode focal reducer (Afanasiev and Moiseev, 2011). The VPHG1200@540 grism was used with a sensitivity maximum at λ 5400 Å providing the full optical range of spectroscopic observations in the wavelength range of 3650–7300 Å with a resolution of about 5 Å. The $1''$-wide slit was oriented at two position angles: at $PA = 115°$ to include the "radio loud" ESE compact emission region (Fig. 2) and at $PA = 158°$ to catch the top of the northern part of the circumnuclear emission loop; the exposure times were 1600 and 800 s respectively. The image quality in spectroscopic observations in 2022 was $2\farcs4$. These long-slit cross sections, together with the cross sections at the position angles $PA = 102°$ and $PA = 0°$, previously obtained with the same instrument and the same grism, were used to measure the fluxes of various emission lines and their ratios for the selected regions at different distances from the center of the galaxy and the line-of-sight velocities of gas and stars.

3. EXCITATION OF THE IONIZED GAS

It has been noted in many previous papers (e.g., Keel and Hummel, 1988) that the strong emission lines in the spectrum of the NGC 2655 nucleus show flux ratios characteristic of the Seyfert type II active nucleus or LINER. Moreover, Keel and Hummel (1988), on the basis of the spectrum of the ESE clump, moderate in the range and the S/N ratio, suspected that the spectrum of the ESE clump located in 1.8 kpc from the nucleus is very similar to the nucleus spectrum in terms of the pattern of flux ratios in the lines. Since the restrictions on the energy of the nucleus did not allow interpreting the ionized gas of the ESE clump as excited by the radiation of the central engine of the active nucleus, it was suggested that the gas excitation source here is a shock wave from the active

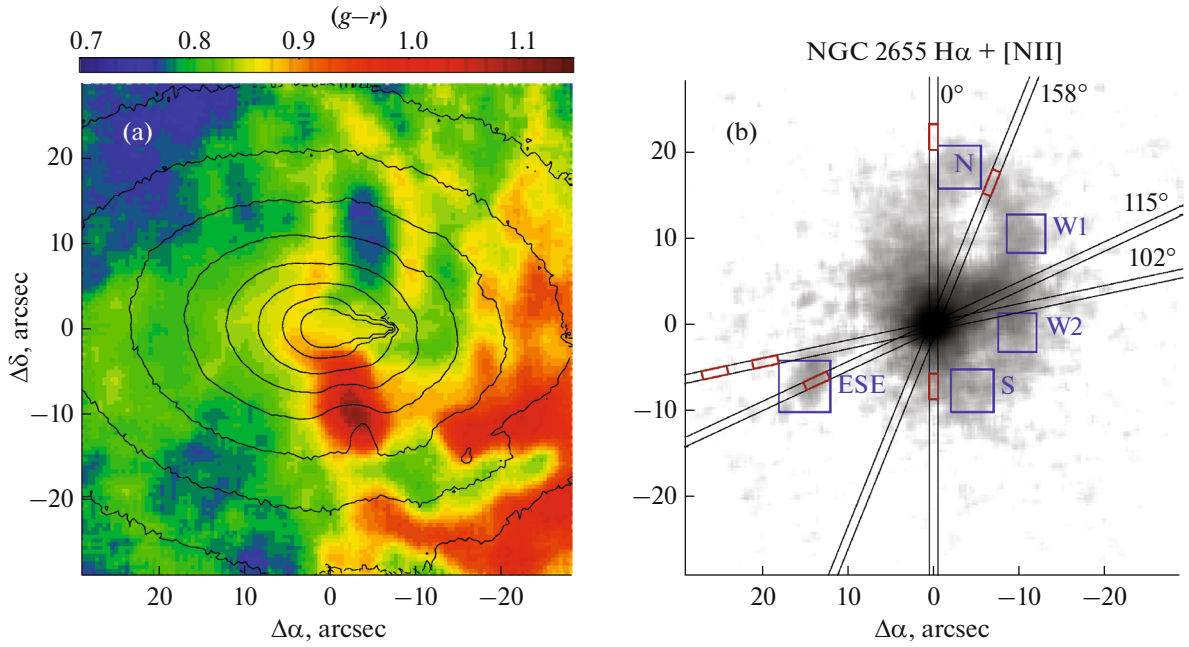

Fig. 2. Central region of the galaxy NGC 2655: (a) in $g–r$ colors from the BASS data, (b) in the narrow Halp filter, the band of which includes the emission lines Hα+ [N II]λ 6548, λ 6583, with the continuum subtracted: according to the data that we obtained with the 2.5-m telescope of the Caucasus Mountain Observatory of SAI MSU. The blue squares mark the parts of the gaseous structure that were selected for further detailed spectroscopic analysis. The black lines show the position of the spectrograph slits and the corresponding position angles. The red rectangles highlight the areas, for which Fig. 3 considers the state of the gas ionization.

nucleus jet which, according to radio interferometry, seems to be turned in the appropriate direction. We obtained quite deep spectra with the 6-m BTA telescope at four different slit orientations. Measurements of the flux ratios of the emission lines in these four spectra showed that the characteristic flux ratio dominated by the highly-excited [O III]λ 5007 line is observed throughout the disk of NGC 2655, not only in the ESE clump but also in the polar central loop (clumps N, W1, and S), and in the regular gaseous disk of NGC 2655 up to a distance of 8 kpc from the center.

Figure 3 shows the diagnostic (BPT) diagrams comparing the ratio of the highly excited [O III]λ 5007 line to the nearest Hβ hydrogen line, and the ratio of the low-excited [N II] λ 6583 line to the neighboring Hα hydrogen line for selected areas of NGC 2655; the BPT diagram was proposed in the paper by Baldwin et al. (1981) for diagnosing a gas ionization source. The red dotted and green dashed lines demarcate the positions of the emission regions excited by young stars (on the left and below the line) from other excitation mechanisms according to the papers by Kauffmann et al. (2003) and Kewley et al. (2001) respectively. Other excitation mechanisms are the ionization either by the power-law spectrum of the active nucleus or by a shock wave: the BPT diagram does not make it possible to distinguish between these two mechanisms. Since the regions under study are located at different distances from the active nucleus, from 1 to 8 kpc, and the line ratios are similar for all the regions, we are obviously dealing with gas excitation by a shock wave. Seven of the eight regions studied contain the gas excited exactly by the shock wave. Although the regions of excitation by the shock wave and the Seyfert nucleus overlap in the BPT diagrams, in this case we are talking about the gas excitation at a large distance from the center, and already Keel and Hummel (1988) have estimated that the radiation energies from the active nucleus of NGC 2655 are not enough even to excite the ESE region at 15″ from the center, not to mention more distant regions. At the $PA = 102°$ orientation, one can see how the shock wave slows down with distance from the center: if we compare the line ratios with the Allen et al. (2008) models, then from the point $r = 20″$ to the point $r = 60″$, the velocity of the shock wave falls down by 150 km s^{-1}. And only one area, at 7 kpc south of the center in $PA = 158°$, is excited by young stars. This compact area is located on the periphery of the outer disk and is also visible in the ultraviolet (Fig. 4). Since the gas in this region is ionized by young stars, we can estimate its metallicity from the strong line flux ratios calibrated using the H II region spectra modeled in detail. We used two popular sources of such calibrations and obtained estimates for the oxygen abundance in the gas for NGC 2655: $12 + \log(O/H) = 8.58 \pm 0.18$ dex by indicator N2 and $12 + \log(O/H) = 8.58 \pm 0.16$ dex by

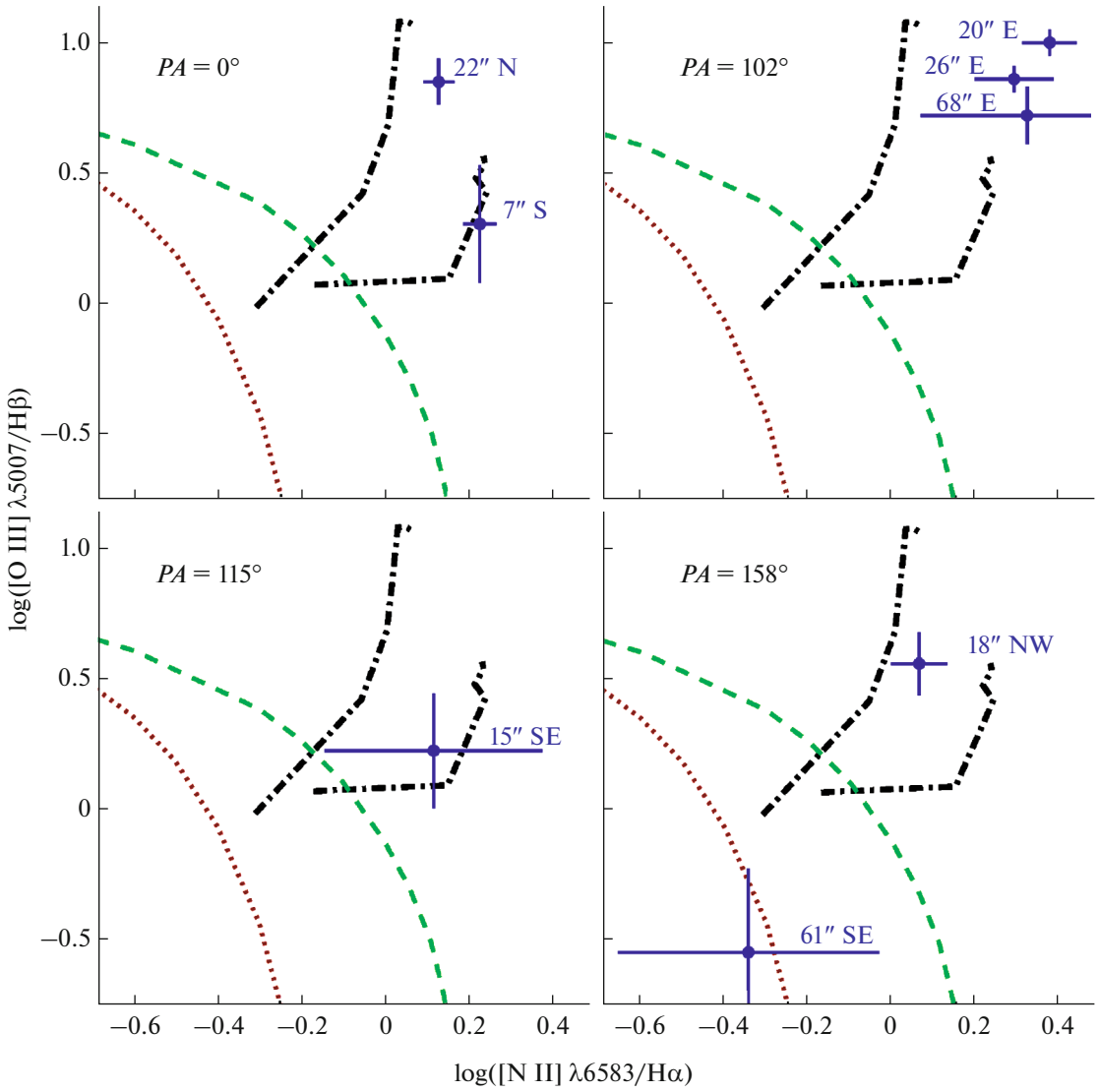

Fig. 3. Diagnostic BPT diagrams for determining the character of excitation of the ionized gas in four spectral cross sections of NGC 2655 with a long slit. The slit orientation is indicated in the upper left corner of each panel. For each point (the emission region), we marked the distance from the galaxy center (along the slit, that is, projected onto the sky plane) and the side of the slit (north or south, west or east). If the emission regions belong to the disk of the galaxy, then these points correspond to physical distances from the nucleus 30″ and 9″ ($PA = 0$) and 24″ and 73″ ($PA = 158°$). The red dotted and green dashed lines demarcate the positions of the emission regions excited by young stars (on the left and below the line) from other excitation mechanisms according to Kauffmann et al. (2003) and Kewley et al. (2001) respectively. The dash-dotted lines show the models of gas excitation by a shock wave—the gas with solar metallicity and the standard electron density $n = 1$ cm^{-3}—from the paper by Allen et al. (2008). Along each polygonal line, the velocity of the shock wave increases from bottom to top, from 200 to 1000 km s^{-1}; the right-hand of the two polygonal lines corresponds to a shock wave propagating in a low-density environment, and the left-hand one corresponds to the dense gas already excited (the shock wave model together with the precursor).

indicator O3N2 (Marino et al., 2013), or $12 + \log(O/H) = 8.71 \pm 0.18$ dex by indicator N2 and $12 + \log(O/H) = 8.79 \pm 0.21$ dex by indicator O3N2 (Pettini and Pagel, 2004). Despite the low accuracy of these estimates, we can still confirm that the metallicity of the gas is approximately solar—and this is on the periphery of the galaxy disk!

4. DETAILED GAS KINEMATICS

Earlier, we repeatedly focused on the polar rotation of the gas in the central region of NGC 2655 (Sil'chenko and Afanasiev, 2004; Sil'chenko et al., 2019). Let us note that the actual pattern of gas kinematics throughout the entire galaxy can be much more complicated than simply turning the rotation plane by

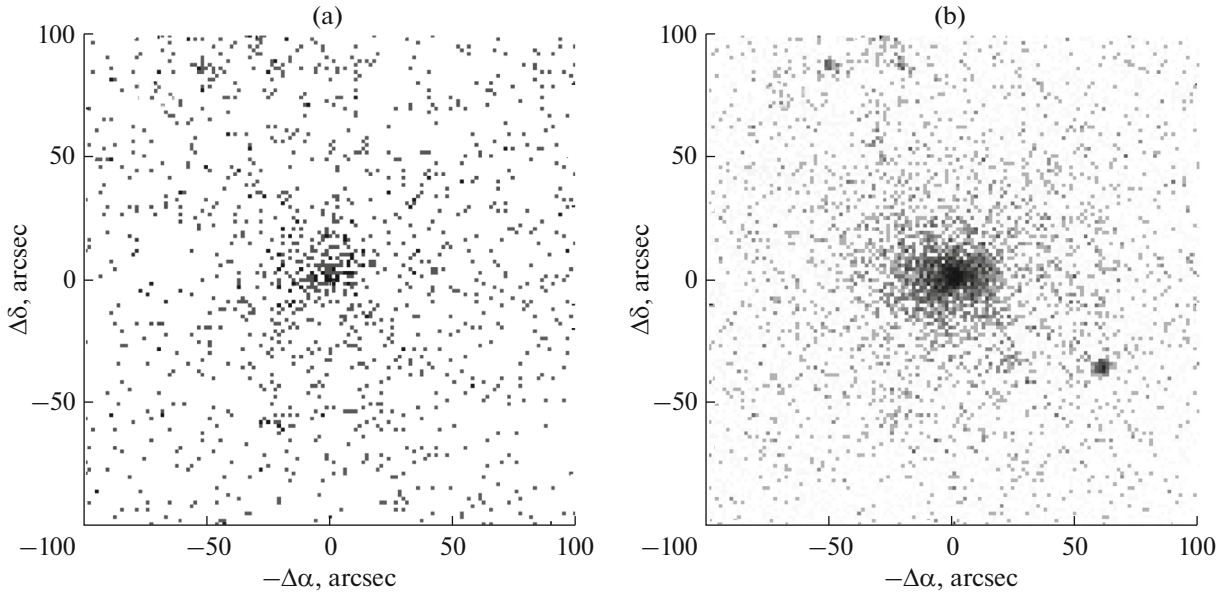

Fig. 4. Ultraviolet maps of NGC 2655 according to the data from the GALEX space telescope: (a) the map in the far ultraviolet, $\lambda \approx 1500$ Å, (b) the map in the near ultraviolet, $\lambda \approx 2300$ Å.

90°. Thus, neutral hydrogen outside the stellar disk rather rotates in a circular manner according to the apparent orientation of the H I disk, with a kinematic major axis close to $PA = 110°$; Sparke et al. (2008) proposed a model with a smooth turn of the gaseous disk, as it approaches the center of the galaxy. Our data on the ionized gas in the outermost regions of the disk, at $R > 40''$, also seem to agree with the stellar kinematics (Sil'chenko et al., 2019). However, the abundance of details in the distribution of the surface brightness of the emission lines in Fig. 2 rather indicates not a smooth curvature of the gaseous disk but the presence of several gas subsystems with different kinematics on the line of sight. This last hypothesis is also consistent with the shock excitation of the gas throughout the disk of NGC 2655.

Using the benefit of rather high spectral resolution of our data obtained with the Fabry–Perot scanning interferometer, in the second approach to their analysis, we decided to take a closer look at the line profiles, specifically, the [O III]λ 5007 emission line profiles, in the narrow range, around which the spectrum of the ionized gas was scanned over the entire body of NGC 2655 with the Fabry–Perot interferometer. The profiles appeared to be complex and multi-component. Figure 5 presents the examples of the Gaussian analysis[2] of these profiles for the loop areas marked as N, W1, W2, and S in Fig. 2. In each region, we can distinguish at least two components with different line-of-sight velocities. In the N and S regions, the stronger components correspond to the polar rotation of the loop; but there are also weak components close to the systemic velocity of the galaxy, 1400 km s^{-1}, expected from the gas on the minor axis of the disk. Obviously, the weak components correspond to the rotation of the gas lying in the plane of the stellar disk, whose isophote major axis (the line of nodes) approximately corresponds to the west–east direction.

For a "radio loud" ESE emission region located at 15″ (1.8 kpc) southeast of the nucleus, Fig. 6 shows the results of the Gaussian analysis of three lines: oxygen according to the Fabry–Perot data and hydrogen, and a nitrogen doublet according to the long-slit spectroscopy data. Although the weak component is measured with low accuracy, but for all three lines it occurs that in the region there is the gas with a line-of-sight velocity of about 1700 km s^{-1}; it is by 300 km s^{-1} greater than the systemic velocity of the galaxy. The gas with a similar velocity is observed at the southwestern edge of the gaseous disk according to the Fabry–Perot (Sil'chenko et al., 2019) data, and this velocity does not correspond to any circular rotation model. Apparently, regarding the ESE clump, the issue is about a compact remnant of a satellite that hit the NGC 2655 disk at a high velocity of 400–500 km s^{-1} almost perpendicular to the stellar disk. The whole configuration with a destroyed companion and a polar circumnuclear loop resembles in appearance the destroyed companion Sgr stretched into a polar flow in our

[2] Let us note that although the FPI instrumental profile differs from the Gaussian one and is described by the Voigt profile and, in the case of the given FPI with a relatively low resolution, the observed line profiles differ little from the Gaussian one which can be clearly seen in Fig. 5.2.

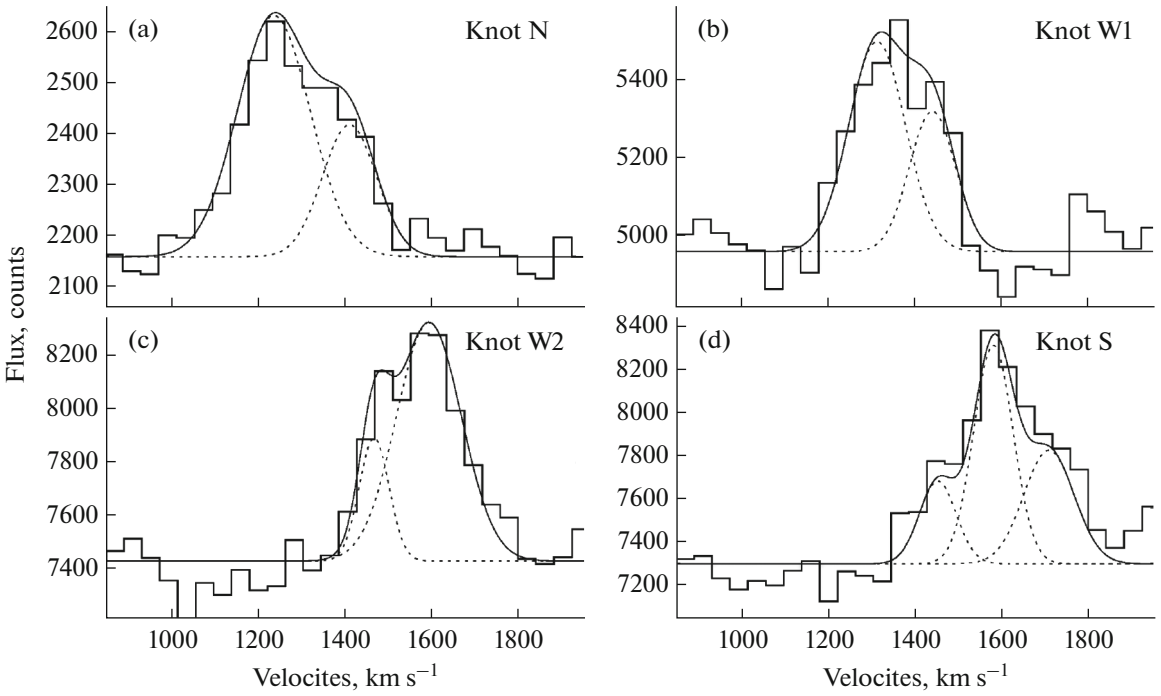

Fig. 5. Gaussian analysis of the [O III] λ 5007 emission line profile for four compact emission regions indicated in Fig. 2 as N, W1, W2, and S—panels (a), (b), (c), and (d) respectively. The first three regions show the presence of two kinematic components each with velocities of 1196 ± 12 and 1371 ± 16 km s^{-1} (N), 1273 ± 33 and 1401 ± 37 km s^{-1} (W1), 1560 ± 6 and 1431 ± 6 km s^{-1} (W2) respectively. The southern clump shows three velocity components: 1539 ± 11, 1667 ± 32, and 1410 ± 120 km s^{-1}.

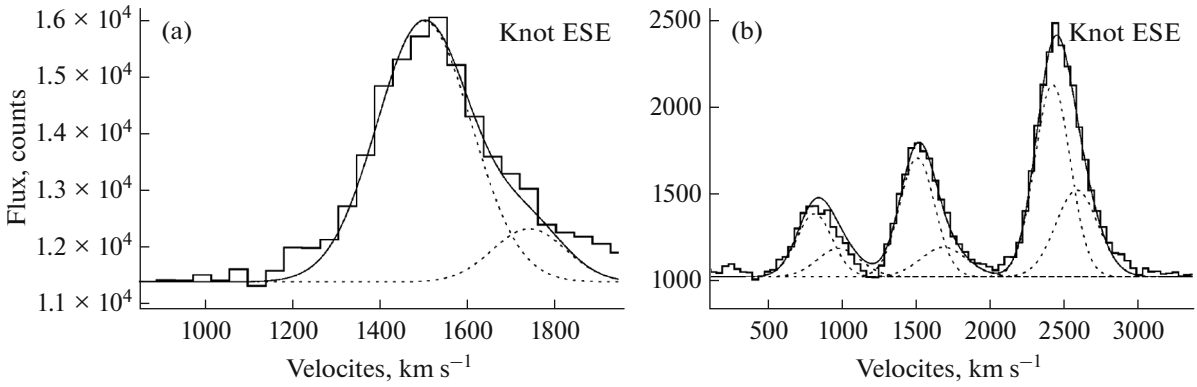

Fig. 6. Gaussian analysis of the emission line profiles for the ESE clump: the [O III] λ 5007 profile according to Fabry–Perot data gives the velocities 1499 ± 99 and 1737 ± 377 km s^{-1} (a), according to the data of the long-slit cut, the gas velocities along the Hα profile are equal to 1517 ± 35 and 1730 ± 295 km s^{-1}, and according to the doublet profile of once ionized nitrogen—1490 ± 36 and 1677 ± 138 km s^{-1} (b). The line-of-sight velocity scales are given for the [O III] λ 5007 and Hα lines respectively.

Milky Way (Ibata et al., 2001; Laporte et al., 2018). And the NGC 2655 own gas, which was "hit" in the center by the fallen companion, should have lost momentum in the shock wave and fell onto the nucleus; perhaps, this is what fuelled the current activity of the nucleus.

5. DISCUSSION

5.1. Structure and Stellar Kinematics of NGC 2655

NGC 2655 is a giant early-type disk galaxy. It is generally believed that such galaxies should have a very large dominant bulge. A detailed morphological anal-

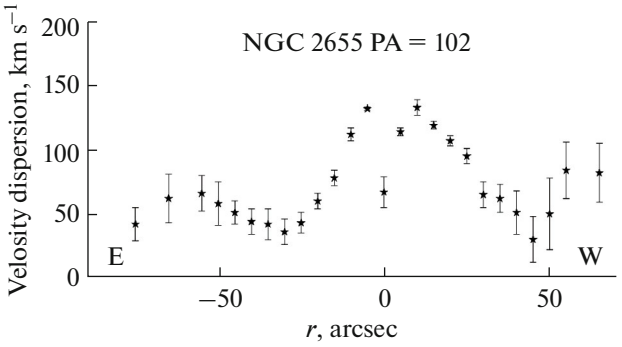

Fig. 7. Velocity dispersion profile of stars in the cross section $PA = 102°$ according to long-slit spectroscopy data.

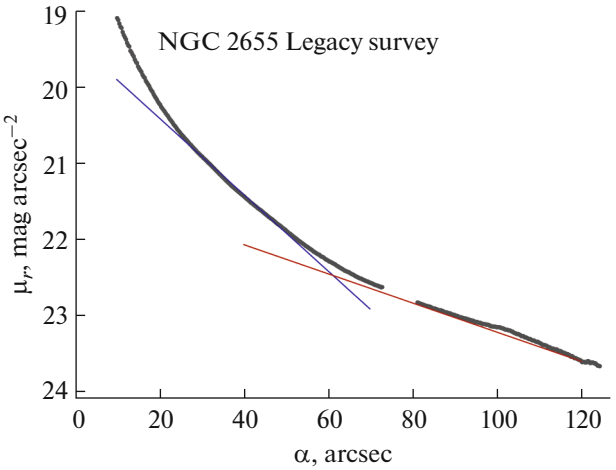

Fig. 8. Azimuthally averaged surface brightness profile of NGC 2655 from the BASS survey data with two inscribed exponential segments $\mu_r = 19.4 + 1.086R''/21.6''$ in the interval $R = 26''–50''$ and $\mu_r = 21.3 + 1.086R''/56.5''$ in the interval $R = 70''–120''$.

ysis and decomposition of the galaxy image into components undertaken by an experienced Finnish team of photometric observers as part of the S4G survey of galaxies (Sheth et al., 2010) showed that the disk contributes no more than 42% to the infrared luminosity (and, obviously, to the stellar mass) (Salo et al., 2015). According to the performed decomposition, the exponential disk begins to dominate in the galaxy at the radius $R > 50''$; while closer to the center, the surface brightness profile consists of the summed contributions of the bulge and bar. Why have the Salo et al. (2015) team decided that NGC 2655 has a bar, even though the galaxy is not classified as SB in any catalog? This is due to the fact that the major axis orientation of the isophotes of the inner components—the bulge, $PA = 82°$, and the bar, $PA = 85\overset{\circ}{.}6$,—is different from the orientation of the outermost isophote disk, $PA = 110°$, which are usually identified with the orientation of the line of nodes. As a result of the NGC 2655 image deprojection undertaken in the S4G survey by the Salo et al. (2015) team exactly with the node line orientation $PA = 110°$, the image of the galaxy with oval internal components has been obtained; the Salo et al. (2015) team considered one of them a triaxial bulge, and the other is a bar.

We do not agree with this interpretation of the structure of NGC 2655. The fact is that with the SAURON integrated field spectrograph, a two-dimensional map of the line-of-sight velocities of stars was measured and published—the projected velocities of the stellar component rotating in the center of the galaxy on the line of sight (Dumas et al., 2007). We analyzed this velocity field using the tilted ring method and found the node line orientation of the stellar-component rotation plane $PA = 263° \pm 3°$ up to the $25''$ distance from the center. Dumas et al. (2007) obtained $PA = 266° \pm 1°$ with the kinemetry method using the same data. The exact coincidence of the orientations of the photometric and kinematic major axes proves that the stars in the center of NGC 2655 rotate in circular orbits in the axisymmetric potential: the galaxy has no bar.

In fact, the determinant feature of a thin stellar disk is its dynamic coldness: when the rotation velocity is many times greater than the dispersion of stellar velocities. Figure 7 shows the profile of the stellar velocity dispersion that we measured along the cross section with a long slit at $PA = 102°$. The measurements of the stellar kinematic parameters were performed by the cross-correlation method similar to that we used in the paper by Sil'chenko et al. (2019). Already at the radius $R = 30''$, the velocity dispersion of stars drops to 50 km s^{-1}: this is the location, where the thin stellar disk begins to dominate. We have also shown in Fig. 8 the decomposition of the surface brightness profile consistent with the dominance of the disk that is so close to the center: the disk of NGC 2655 has the type III profile, that is, it consists of two exponential segments, an inner one with a smaller characteristic scale and an outer (which was also found in the S4G survey) with a greater one.

Thus, we can say that NGC 2655 has two exponential disks: they have different scalelengths, but they also have different orientations of the isophote major axis. And along with this, the orientation of the major axis of the internal isophote is supported by kinematics: as the analysis of the two-dimensional velocity field shows, this is indeed the line of nodes of the circular rotation plane. As for the outer disk, for which the orientation of the photometric major axis $PA = 110°$ was found in the S4G survey, here we cannot properly compare with the orientation of the kinematic major axis: there is no two-dimensional stellar velocity field. But we have long-slit cuts in different slit

orientations. Figure 9 compares the line-of-sight velocity profiles of the stellar component in the slit orientations $PA = 102°$ and $PA = 115°$. We can note that at the radius $R = 40''$, the projected rotation velocity on the line of sight is larger at $PA = 115°$ than at $PA = 102°$. This means that the kinematic major axis in the outer stellar disk is closer to $PA = 115°$ than to $PA = 102°$ which excludes the orientation node line $PA = 83° \pm 3°$ found for the inner disk. At the same time, the photometric major axis $PA = 110°$ can be the orientation of the line of nodes of the outer disk, our kinematic cross sections with a long slit do not exclude this. It appears that the internal and external rotation axes of the stellar disk of NGC 2655 are inclined to each other, in other words, it is a multi spin galaxy.

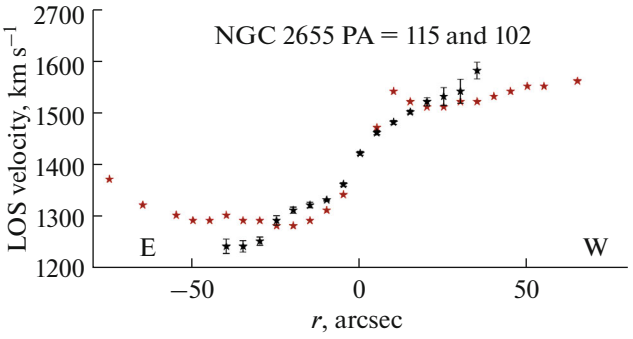

Fig. 9. Radial velocity profile of the stellar component along two orientations close to the photometric major axis: the red asterisks are for $PA = 102°$, the black asterisks are for $PA = 115°$.

5.2. Origin of Gas in NGC 2655

The orientations of the huge disk of neutral hydrogen and the outer stellar disk in NGC 2655 are consistent with each other both spatially and kinematically. Previously, Sparke et al. (2008) noted that two billion solar masses of gas is too much for one minor merging, and several such events are needed (but with the same orientation of the infall orbits, because all the gas rotates in the same plane). Now we understand that these multiple minor mergers should have brought not only several billion solar masses of gas, but also several billion solar masses of stars for the outer stellar disk of NGC 2655, which makes the supposed multiple minor merging a quite tremendous—and incredible—event. In contrast to Sparke et al. (2008), we conclude that the outer gaseous disk lies within the outer stellar disk, and even star formation is taking place in some places in it: in the southern edge we detect the corresponding emission of gas excited by young stars, and the northern "arc" shows an excess of ultraviolet (Fig. 4). The metallicity of the gas in this outer disk is solar, which is atypical for dwarf galaxies that Sparke et al. (2008), have suggested as the source of NGC 2655 gaseous disk. The entire external configuration of the galaxy resembles a classical large disk of a spiral galaxy, which, according to modern concepts, is "cumulated" over billions years by smooth external accretion of cold gas (Tacconi et al., 2020), albeit from a source undefined at a global scale.

But minor merging certainly took place in NGC 2655. It also brought along a noticeable amount of the gas with kinematics significantly different from the regular rotation of the outer disk. Apparently, the companion fell onto the galaxy almost vertically, and now, within two kiloparsecs from the center, we observe the remnants of a broken companion as a circumpolar loop—the picture is very similar to Sagittarius torn apart by the Milky Way. But in this case, there was much more gas in the fallen companion. The gas of the vertically falling companion hit the gaseous disk of NGC 2655 being in regular rotation, and this collision inevitably resulted in the development of shock fronts. The shock wave not only excited the gas in the polar loop, it "ran" outward across the large galactic gaseous disk. At distances of up to 8 kpc from the center, we observe the gas of the large disk excited by this shock wave, although, the kinematics of this gas to the east of the nucleus is little affected and exhibits rotation consistent with that of the stellar disk. If the shock wave propagated at an average velocity of 1000 km s^{-1}, then the impact could have taken place approximately 10^7 years ago.

ACKNOWLEDGMENTS

We obtained the observed data partially with the unique scientific installation—the Big Telescope Alt-azimuth of SAO RAS. Observations with the SAO RAS telescopes are supported by the Ministry of Science and Higher Education of the Russian Federation. Upgrading of the instruments is carried out within the framework of the "Science and Universities" national project. In our paper, we used the data from the NED Extragalactic Database (NASA/IPAC) operated by the Jet Propulsion Laboratory and the California Institute of Technology under the contract to NASA. We used the public data from the Hubble Space Telescope taken from the Hubble Legacy Archive (the collaboration of the Telescope Science Institute, the Space Telescope European Coordinating Facility, and the Canadian Astronomy Data Centre), the data from the GALEX space telescope (NASA Galaxy Evolution Explorer) operated by the California Institute of Technology under the NASA contract No. NAS5-98034. The GALEX data comes from the MAST (Mikulski Archive for Space Telescopes) public archive maintained by the NASA Space Office under grant NNX13AC07G and other grants. The optical photometry data were provided by the Legacy Survey service based on the BASS survey data. BASS is a key project of the Chinese Telescope Access Program (TAP) funded by the National Astronomical Observatories of China, the Chinese Academy of Sciences (the Strategic Priority Research Program

"Emergence of Cosmological Structures", grant No. XDB09000000), and the Special Fund for Astronomy from the Ministry of Finance. BASS is also supported by the External Cooperation Program of the Chinese Academy of Sciences (grant no. 114A11KYSB20160057) and the National Natural Science Foundation of China (grants no. 12120101003 and no. 11433005).

FUNDING

Spectroscopic observations and data analysis were supported by the grant from the Russian Science Foundation no. 22-12-00080. Photometric observations in narrow filters were supported by the RFBR grant no. 20-02-00080.

CONFLICT OF INTEREST

The authors declare no conflict of interest regarding the publication of this paper.

REFERENCES

1. V. L. Afanasiev and A.V. Moiseev, Baltic Astronomy **20**, 363 (2011).
2. M. G. Allen, B. A. Groves, M. A. Dopita, et al., Astrophys. J. Suppl. **178** (1), 20 (2008).
3. J. A. Baldwin, M. M. Phillips, and R. Terlevich, Publ. Astron. Soc. Pacific **93**, 5 (1981).
4. A. Y. K. Bouquin, A. Gil de Paz, J. C. Muñoz-Mateos, et al., Astrophys. J. Suppl. **234** (2), article id. 18 (2018).
5. B. Catinella, A. Saintonge, S. Janowiecki, et al., Monthly Notices Royal Astron. Soc. **476** (1), 875 (2018).
6. L. Cortese, B. Catinella, R. H. W. Cook, and S. Janowiecki,Monthly Notices Royal Astron. Soc. **494** (1), L42 (2020).
7. T. A. Davis, K. Alatalo, M. Sarzi, et al., Monthly Notices Royal Astron. Soc. **417** (2), 882 (2011).
8. G. Dumas, C. G. Mundell, E. Emsellem, and N. M. Nagar, Monthly Notices Royal Astron. Soc. **379** (4), 1249 (2007).
9. A. M. Garcia, Astron. and Astrophys. Suppl. **100**, 47 (1993).
10. M.Grossi, S. di Serego Alighieri, C. Giovanardi, et al., Astron. and Astrophys. **498** (2), 407 (2009).
11. J. E. Gunn and J. R. Gott, III, Astrophys. J. **176**, 1 (1972).
12. L. C. Ho and J. S. Ulvestad, Astrophys. J. Suppl. **133** (1), 77 (2001).
13. E. P. Hubble, *Realm of the Nebulae* (Yale University Press, New Haven, 1936).
14. W. K. Huchtmeier and O. G. Richter, Astron. and Astrophys. **109**, 331 (1982).
15. E. Hummel, J. M. van der Hulst, and J. M. Dickey, Astron. and Astrophys. **134**, 207 (1984).
16. R. Ibata, M. Irwin, G. F. Lewis, and A. Stolte, Astrophys. J. **547** (2), L133 (2001).
17. I. Y. Katkov, A. Y. Kniazev, and O. K. Sil'chenko, Astron. J. **150** (1), article id. 24 (2015).
18. G. Kauffmann, T. M. Heckman, C. Tremonti, et al., Monthly Notices Royal Astron. Soc. **346** (4), 1055 (2003).
19. W. C. Keel and E. Hummel, Astron. and Astrophys. **194**, 90 (1988).
20. L. J. Kewley, M. A. Dopita, R. S. Sutherland, et al., Astrophys. J. **556** (1), 121 (2001).
21. K. Kuijken, D. Fisher, and M. R. Merrifield, Monthly Notices Royal Astron. Soc. **283** (2), 543 (1996).
22. C. F. P. Laporte, K. V. Johnston, F. A. Gómez, et al., Monthly Notices Royal Astron. Soc. **481** (1), 286 (2018).
23. R. B. Larson, B. M. Tinsley, and C. N. Caldwell, Astrophys. J. **237**, 692 (1980).
24. B. M. Lewis and R. D. Davies, Monthly Notices Royal Astron. Soc. **165**, 213 (1973).
25. R. A. Marino, F. F. Rosales-Ortega, S. F. Sánchez, et al., Astron. and Astrophys. **559**, id. A114 (2013).
26. A. V. Moiseev and O. V. Egorov, Astrophysical Bulletin **63**, 181 (2008).
27. M. Pettini and B. E. J. Pagel, Monthly Notices Royal Astron. Soc. **348** (3), L59 (2004).
28. H. Salo, E. Laurikainen, J. Laine, et al., Astrophys. J. Suppl. **219** (1), 4 (2015).
29. P. Serra, T. Oosterloo, R. Morganti, et al., Monthly Notices Royal Astron. Soc. **422** (3), 1835 (2012).
30. W. W. Shane and N. Krumm, IAU Symp. **100**, pp. 105–106 (1983).
31. N. Shatsky, A. Belinski, A. Dodin, et al., in Proc. All-Russian Conf. on Ground-Based Astronomy in Russia. 21st Century, Nizhny Arkhyz, Russia, 2020, Ed. by I. I. Romanyuk, I. A. Yakunin, A. F. Valeev, and D. O. Kudryavtsev, pp. 127–132 (IP Reshenilenko P.A., Pyatigorsk, 2020).
32. K. Sheth, M. Regan, J. L. Hinz, et al., Publ. Astron. Soc. Pacific **122** (898), 1397 (2010).
33. O. K. Sil'chenko and V. L. Afanasiev, Astron. J. **127** (5), 2641 (2004).
34. O. K. Sil'chenko and A. N. Burenkov, Astron. and Astrophys. **233**, 314 (1990).
35. O. K. Sil'chenko, A. V. Moiseev, and O. V. Egorov, Astrophys. J. Suppl. **244** (1), article id. 6 (2019).
36. L. S. Sparke, G. van Moorsel, P. Erwin, and E. M. H. Wehner, Astron. J. **135** (1), 99 (2008).
37. L. J. Tacconi, R. Genzel, and A. Sternberg, Annual Rev. Astron. Astrophys. **58**, 157 (2020).
38. Y. Terashima, N. Iyomoto, L. C. Ho, and A. F. Ptak, Astrophys. J. Suppl. **139** (1), 1 (2002).

Translated by N. Oborina